

# DexSim2Real<sup>2</sup>: Building Explicit World Model for Precise Articulated Object Dexterous Manipulation

Taoran Jiang\*, Liqian Ma\*, Yixuan Guan, Jiaojiao Meng, Weihang Chen, Zecui Zeng, Lusong Li, Dan Wu, Jing Xu *Member, IEEE*, Rui Chen *Member, IEEE*

**Abstract**—Articulated object manipulation is ubiquitous in daily life. In this paper, we present DexSim2Real<sup>2</sup>, a novel robot learning framework for goal-conditioned articulated object manipulation using both two-finger grippers and multi-finger dexterous hands. The key of our framework is constructing an explicit world model of unseen articulated objects through active one-step interactions. This explicit world model enables sampling-based model predictive control to plan trajectories achieving different manipulation goals without needing human demonstrations or reinforcement learning. It first predicts an interaction motion using an affordance estimation network trained on self-supervised interaction data or videos of human manipulation from the internet. After executing this interaction on the real robot, the framework constructs a digital twin of the articulated object in simulation based on the two point clouds before and after the interaction. For dexterous multi-finger manipulation, we propose to utilize eigengrasp to reduce the high-dimensional action space, enabling more efficient trajectory searching. Extensive experiments validate the framework’s effectiveness for precise articulated object manipulation in both simulation and the real world using a two-finger gripper and a 16-DoF dexterous hand. The robust generalizability of the explicit world model also enables advanced manipulation strategies, such as manipulating with different tools.

**Index Terms**—Dexterous manipulation, Sim2Real, articulated object, world model

## I. INTRODUCTION

ARTICULATED object manipulation is a fundamental and challenging problem in robotics. Compared with pick-and-place tasks, where only the start and final poses of robot end effectors are constrained, articulated object manipulation requires the robot end effector to move along certain trajectories, making the problem significantly more complex. Most existing works utilize a neural network to learn the correlation between object states and correct actions, and employ reinforcement learning (RL) and imitation learning (IL) to train the neural network [1]–[3]. However, since the state distribution of articulated objects is higher-dimensional and more complex

\*Taoran Jiang and Liqian Ma contributed equally to this work. Corresponding author: Rui Chen chenrui@tsinghua.edu.cn

Taoran Jiang, Liqian Ma, Yixuan Guan, Jiaojiao Meng, Weihang Chen, Dan Wu, Jing Xu, Rui Chen are with the Department of Mechanical Engineering, Tsinghua University, Beijing 100084, China.

Taoran Jiang is also with School of Automatic Science and Electric Engineering, Beihang University, Beijing 100191, China.

Liqian Ma is also with the Institute for Robotics and Intelligent Machines (IRIM), Georgia Institute of Technology. This work was done while he was affiliated with the Department of Mechanical Engineering, Tsinghua University.

Zecui Zeng, Lusong Li are with JD Explore Academy, Beijing, China.

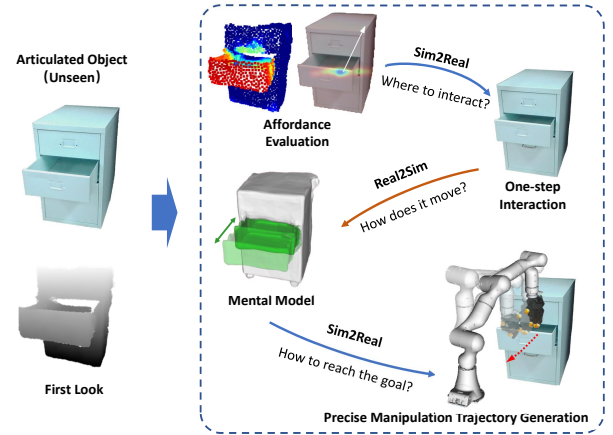


Fig. 1. DexSim2Real<sup>2</sup> is a robot learning framework for precise goal-conditioned articulated object manipulation with two-finger grippers and multi-finger dexterous hands in the real world. It builds the mental model of the unseen target object through one-step active interaction and uses the model to generate a long-horizon manipulation trajectory.

than that of rigid objects, it is difficult for the neural network to learn such correlation, even with hundreds of successful demonstrations and millions of interactions [4], [5].

For humans, manipulation involves not only action responding to perception, as is the case with policy networks, but also motor imagery and mental simulation, that humans can imagine the action consequences before execution and plan the action trajectory accordingly [6]. To model the world more accurately, humans can actively interacting with the environment, changing its states and gathering additional information, which is named as *interactive perception* [7], [8].

In this paper, we propose a robot learning framework called DexSim2Real<sup>2</sup> to achieve precise goal-conditioned manipulation of articulated objects using two-finger grippers and multi-finger dexterous hands, where we use a physics simulator as the *mental model* of robots. Fig. 1 provides a brief overview of our framework. Given a single-view RGBD image of the articulated object at its initial state as input, the framework first learns an affordance estimation network from self-supervised interaction in simulation or egocentric videos of human-object interactions. The network predicts a one-step motion of the robot end effector. The reason why we first learn the affordance is that affordance estimation is only attributed to the object and can better generalize to novel objects. Also the one-step interaction does not require fine manipulation of the dexterous hand. Next, we execute the predicted action on the real robot to change the object’s state and capture another

RGBD image after the interaction. Then, we train a module to construct an explicit world model of the articulated object. We transform the two RGBD images into two point clouds and generate a digital twin of the articulated object in simulation. Finally, using the explicit world model we have built, we utilize sampling-based model predictive control (MPC) to plan a trajectory to achieve goal-conditioned manipulation tasks.

While dexterous manipulation with multi-finger hands enables more flexible, efficient and robust manipulation, the high-dimensional action space presents significant challenges for MPC. To handle this problem, we propose to employ eigen-grasp [9] to reduce the operational dimensions of the dexterous hand, enabling more efficient and successful searching. While eigen-grasp has been widely studied for robot grasping [10]–[12], its application in dexterous manipulation remains under-explored. Since our method constructs an explicit world model of the articulated object, we can accurately predict its motion upon contact with the dexterous hand. This allows us to search for a feasible dexterous manipulation trajectory.

This article is an extension of our previous ICRA work: Sim2Real<sup>2</sup> [13]. There are two main additional contributions in this work:

(1) We broaden the framework’s scope from manipulation with two-finger gripper to multi-finger dexterous manipulation. To address the challenge introduced by the high-dimensional action space of the dexterous hand, we propose to utilize eigen-grasp to reduce the dimension, leading to more efficient and successful manipulation. We conduct extensive experiments both in simulation and on a real robot to validate our method’s effectiveness for dexterous manipulation and the usefulness of its different modules.

(2) In our previous work, we use self-supervised interaction in simulation to generate training data for affordance estimation, which requires interactable 3D assets which is still inadequate currently. To eliminate such dependency and enhance our framework’s scalability, we propose to learn the affordance from egocentric human manipulation videos, which are large-scale and freely accessible. However, since trajectories in videos are in 2D pixel space, we propose a spatial projection method to generate 3D robot motions from 2D trajectory predictions.

The remainder of this paper is structured as follows: Related works are reviewed in Section II. Our proposed robot learning framework is detailed in Section III. Experimental setup and results are presented in Section IV. Finally, conclusions, limitations, and future directions are discussed in Section V.

## II. RELATED WORK

### A. Dexterous Manipulation

Compared with two-finger grippers, multi-finger dexterous hands can manipulate a broader range of objects with more human-like dexterous actions [14]. Traditional model-based approaches formulate dexterous manipulation as a planning problem and generate trajectories through search and optimization [15]–[18]. These methods require accurate 3D shapes of the manipulated object and the hand, which limits their applicability to unseen objects.

In contrast, data-driven methods learn manipulation policies through imitation learning and reinforcement learning [19]–[24]. In [21], a single-camera teleoperation system is developed for 3D demonstration trajectory collection, significantly reducing the equipment cost. Nevertheless, the time consuming nature of human demonstration and the space required for scene setup still limits the scalability of imitation learning. RL eliminates the need for demonstrations and leads to better scalability. Most existing RL methods learn a policy, which directly maps the observation into the joint angles of the dexterous hand [22]–[24]. However, the high-dimensional action space slows the learning efficiency and usually results in uncommon hand motion which cannot be executed on real robot hands. In [12], eigen-grasps [9] are used to reduce the dimension of the action space for functional grasping. Experimental results show that the utilization of eigen-grasp can lead to more stable and physically realistic hand motion for robot grasping. However, more advanced manipulation policies are not studied in this work.

In our work, we combine the advantages of model-based methods and data-driven methods by first learning a generalizable world model construction module and then using the model to search for a feasible trajectory for dexterous manipulation. Furthermore, we adopt eigen-grasps to accelerate the searching process and generate more reasonable hand motions that can be directly executed on real robots.

### B. World Model Construction

Building an accurate and generalizable transition model of the environment capable of reacting to agent interactions has been a long-standing problem in optimal control and model-based RL [25], [26]. Some existing methods model the dynamic system in a lower-dimensional state space, reducing computation and simplifying the transition model [27]–[29]. However, this approach discards the environment’s spatial structure, which limits the model’s generalizability to novel interactions.

With increasing computational power and large network architectures, image-based and video-based world models have gain increasing attention [30]–[33]. In [33], a U-Net-based video diffusion model is used to predict future observation video sequence from the past observations and actions. While it shows great ability to emulate real-world manipulation and navigation environments, it requires an extremely large-scale dataset and computational resources for network training, because the network contains minimal knowledge prior of the environment. Additionally, the inference speed of the large network limits its feasibility for MPC.

In our work, we focus on articulated object manipulation, so we introduce the knowledge prior of the environment by using an explicit physics model. Therefore, we are able to decrease the number of samples required for model construction to 1. Moreover, the explicit physics model’s generalizability guarantees that while we only use a simple action to collect the sample, the built model can be used for long-horizon complex trajectory planning composed of unseen robot actions.

### C. Affordance Learning

In the context of articulated objects, affordances dictate how their movable parts can be interacted by a robot to achieve a desired configuration, which provides a valuable guide for articulated object manipulation. Therefore, affordance learning has been widely studied in the literature. Deng et al. built a benchmark for visual object affordance understanding by manual annotation [34]. Cui et al. explored learning affordances using point supervision [35]. While these supervised learning methods can yield accurate affordance predictions, the cost of the manual annotation process limits their scalability.

Another line of research focuses on learning the affordances through interactions in simulation [1], [3], [36]. Where2act [36] first collects random offline interaction trajectories and then samples online interaction data points for training data generation to facilitate affordance learning. However, the key bottleneck of simulation-based methods is the requirement for 3D articulated object assets that can be accurately interacted with and simulated. Unfortunately, most existing 3D object datasets only include static CAD models, which cannot be used for physics simulation [37], [38].

Videos of human-object interactions are free, large-scale, and diverse, making them an ideal data source for robot learning [39]–[41]. In VRB [40], the contact point and post-contact trajectory are first extracted from videos of human manipulation, and then they are used to supervise the training of the affordance model. However, the predicted affordance is only 2D coordinate and direction in the image, which cannot be directly used for robot execution. Therefore, we propose to generate the robot interaction direction in the 3D physical space by synthesizing a virtual image from the RGBD data and computing the 3D robot motion as the intersection of the 2 VRB predictions in the 3D space.

### D. Sim2Real for Robot Learning

Physics simulation plays a pivotal role in manipulation policy learning, offering large-scale parallelism, reduced training costs, and avoidance of potential damage to robots and researchers [42]–[45]. Most existing methods utilize RL for policy learning in simulation and then deploy the learned policy on a real robot [46]–[48]. DexPoint [23] utilizes the concatenation of observed point clouds and imagined hand point cloud as inputs and learns dexterous manipulation policy. However, since the neural network does not contain any prior knowledge of the environment, a large amount of interaction data is required to improve its accuracy and generalizability. In contrast, we propose to first build the explicit world model of the target object and employ MPC to generate manipulation trajectories based on the built model of the single object instance. By avoiding the diversity of objects, we substantially reduce the required interactions and improve the manipulation accuracy in the real world.

## III. METHOD

The goal of our work is to manipulate articulated objects to specified joint states with various robot-effectors in the real

world, including two-finger grippers and multi-finger dexterous hands. To better align with actual application scenarios, we employ a single depth sensor to acquire a partial point cloud of the object as the observation. Fig. 2 shows an overview of our framework. It consists of three modules: **Interactive Perception** (Section III-A), **Explicit World Model Construction** (Section III-B), **Sampling-based Model Predictive Control** (Section III-C).

A single observation of an articulated object cannot provide enough information to reveal its full structure. For example, when humans first look at a kitchen door, it is hard to tell whether it has a rotating hinge or a sliding hinge. However, after the door is moved, humans can use the information from the two observations to infer the type and location of the hinge. Inspired by this, the **Interactive Perception** module proposes an action to alter the joint state of the articulated object based on learned affordance. This action is then executed on the object in the real world, resulting in two frames of point clouds: one before the interaction and one after.

With the two point clouds, the **Explicit World Model Construction** module (Section III-B) infers the shape and the kinematic structure of the articulated object to construct a digital model. The digital model can be loaded into a physics simulator for the robot to interact with, forming an explicit world model of the environment.

The constructed world model can be used to search for a trajectory of control inputs that change the state of the articulated object from  $s_{\text{initial}}$  to a target state  $s_{\text{target}}$  using **Sampling-based Model Predictive Control**, introduced in Section III-C. With the model of a specific object, we can efficiently plan a trajectory using sampling-based MPC to manipulate the object precisely, rather than learning a generalizable policy.

### A. Interactive Perception

At the beginning, the articulated object is placed statically within the scene, and the robot has only a single-frame observation of it. Understanding the articulation structure and surface geometry of each part of the object from this limited view is challenging. However, by actively interacting with the object and altering its state, additional information can be gathered to enhance the understanding of its structure. It is worth noting that the interaction in this step does not require precision.

To achieve this goal, it is essential to learn to predict the affordance based on the initial single-frame observation. In our work, we first learn the affordance through self-supervised interaction in simulation. However, simulation requires interactable 3D assets, which are still relatively scarce. Therefore, we further study learning affordances from real-world human manipulation videos, which are readily available and large-scale.

1) *Learn from self-supervised interaction in simulation:* By extensively interacting with articulated objects in the simulation, actions that change the state of the articulated object to some extent can be automatically labeled as successful. Using these automatically labeled observation-action pairs, neural networks can be trained to predict candidate actions that can

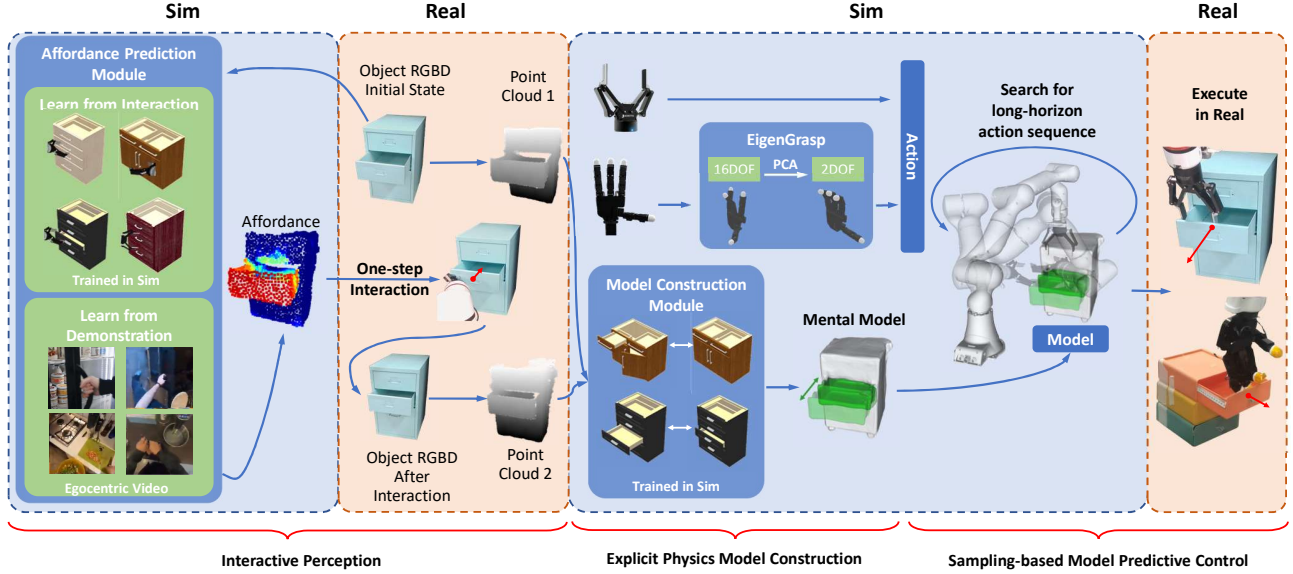


Fig. 2. Overview of the **DexSim2Real<sup>2</sup>** framework. Our framework consists of three phases. (1) Given a partial point cloud of an unseen articulated object, in the **Interactive Perception** phase, we train an affordance prediction module and use it to change the object’s joint state through a one-step interaction. Training data can be acquired through self-supervised interaction in simulation or from egocentric human demonstration videos. (2) In the **Explicit Physics Model Construction** phase, we build a mental model in a physics simulator from the two point clouds. (3) In the **Sampling-based Model Predictive Control** phase, we use the model to plan a long-horizon trajectory in simulation and then execute the trajectory on the real robot to complete the task. For dexterous hands, an eigengrasp module is needed for dimensionality reduction. The eigengrasp module also makes the motion more regular, e.g., it can reduce joint jerk (IV-D).

change the object’s state based on the initial observation of the object.

For affordance learning in this method, we use Where2Act [36]. This algorithm includes an Actionability Scoring Module, which predicts an actionability score  $a_p$  for all points. A higher  $a_p$  indicates a higher likelihood that an action executed at that point will move the part. Additionally, the Action Proposal Module suggests actions for a specific point. The Action Scoring Module then predicts the success likelihood of these proposed actions.

In Where2Act, only a flying gripper is considered, and primitive actions are parameterized by the gripper pose in  $SE(3)$  space. This approach does not account for the robot’s kinematic structure, increasing the difficulty of execution in the real world due to potential motion planning failures. Although this simplification eases the learning process, it complicates real-world execution, as motion planning may not find feasible solutions for the proposed actions.

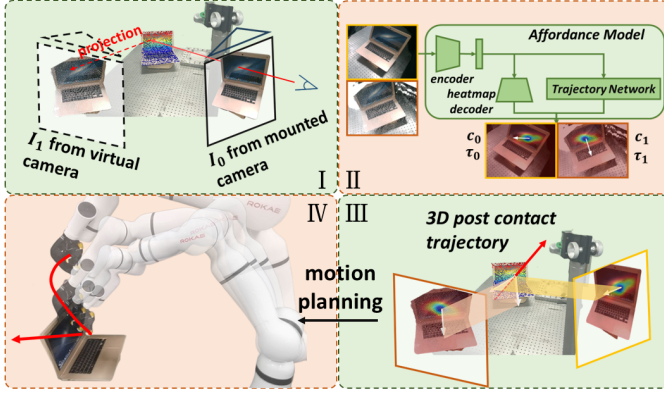
To address this problem, we select  $n_p$  points with the highest actionability scores as candidate points. For each candidate point, we choose  $n_a$  actions with the highest success likelihood scores from the proposed actions. We then use motion planning to attempt to generate joint trajectories for these actions sequentially until a successful one is found. Empirically, we find that this method improves the success rate for the motion planner because the action with the highest success likelihood is often outside the robot’s dexterous workspace.

2) *Learn from real-world egocentric demonstrations*: Acquiring 3D affordance representations through self-supervised interactions in simulation has shown promise as it doesn’t rely on labeled data. However, certain limitation exists: the success of this method hinges on interactive models in simulation. Un-

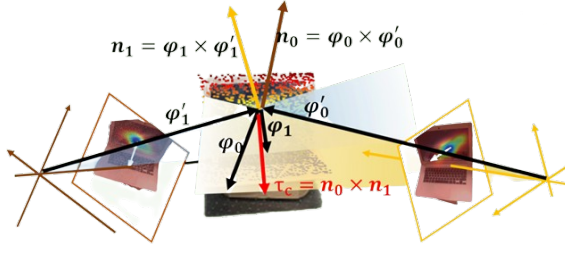
fortunately, the availability of simulated datasets for articulated objects is limited, hindering the generation of training data.

To address this limitation, we propose another approach that leverages real-world egocentric videos of humans interacting with objects. This complementary data source allows us to overcome the limitations of simulation-based learning and broaden the scope of our affordance representation system. Specifically, we utilize the Vision-Robotics Bridge (VRB) [40] to predict the affordance of articulated objects. VRB introduces an innovative affordance model that learns from human videos. It extracts the contact region and post-contact wrist trajectory of the video. These cues serve as supervision signals for training the affordance model. Given an RGB image of an object as input, the VRB model generates two key outputs: a contact heatmap, highlighting the regions where contact occurs, and a 2D vector representation of the post-contact trajectory within the image. Both of these two outputs are within 2D space. However, for effective interaction between robots and objects in the real world, a 3D manipulation strategy is necessary. To address this issue, we need to convert the 2D affordance generated by the model into valid 3D spatial vector and contact region.

Fig. 3(a) illustrates how we generate a 3D trajectory for real robot manipulation from 2D affordances. Firstly, we capture an RGB image  $I_0$  and a 3D point cloud  $\mathcal{P}_0$  using the mounted RGBD camera,  $H_0 \in \mathbb{R}^{4 \times 4}$  is its relative transformation matrix respect to the robot coordinate system. Secondly, we set a virtual camera, the relative transformation matrix of which is  $H \in \mathbb{R}^{4 \times 4}$ . Since the depth of each pixel in  $I_0$  is known, we can generate the virtual RGB image  $I_1$  by image wrapping. Thirdly, we use  $I_0$  and  $I_1$  as the input of the affordance model and generate contact points  $c_0 = (u_0, v_0)$ ,  $c_1 = (u_1, v_1)$



(a)



(b)

Fig. 3. (a)Framework of generating real robot manipulation trajectory from 2D affordances. (b)Calculation method of 3D post contact vector generation.

and post-contact trajectories  $\tau_0 = (u'_0 - u_0, v'_0 - v_0)$  and  $\tau_1 = (u'_1 - u_1, v'_1 - v_1)$ . The camera intrinsic matrix is  $\mathbf{K}$ , the contact point in the mounted camera frame is  $\mathbf{p}_c \in \mathbb{R}^3$ , the 3D post contact vector in the camera frame is  $\tau_c \in \mathbb{R}^3$ . Fourthly, we respectively calculate the 3D contact point and post contact vector. We use contact point  $c_0$  to acquire 3D contact point  $\mathbf{p}_c \in \mathbb{R}^3$  in the robot base frame:

$$\mathbf{p}_c = \mathbf{H}_0^{-1} \mathbf{K}^{-1} z_c \begin{bmatrix} u_0 \\ v_0 \\ 1 \end{bmatrix} \quad (1)$$

where  $z_c$  represents the depth of  $\mathbf{p}_c$ . We use camera's intrinsic matrix to transfer  $c_0$  to point in mounted camera frame than use mounted camera's extrinsic matrix to transfer it to the 3D point cloud  $\mathbf{p}_c$ .

However, generating 3D post-contact vector from 2D information can be comparatively difficult. we can regard the 2D post contact vectors as the projection of 3D vector on their image planes. For each 2D vector, there exists countless 3D vectors whose projection on the image plane is the same as the 2D vector. These vectors are all distributed in a same "projection plane". Given that two different 2D vectors have been generated, we can use the intersection lines of two planes to represent the 3D post contact vector.

Specifically, our method of calculating 3D post contact vector is shown in Fig. 3(b). We respectively denote the projection plane of  $I_0$  and  $I_1$  as  $S_0$  and  $S_1$ . For  $S_0$ , we use  $\varphi_0$  and  $\varphi'_0$  to represent the projection plane.  $\varphi_0$  represents

one possible 3D vector on projection plane  $S_0$ . Its starting point is  $\mathbf{p}_c$ , while its ending point can be calculated with:

$$\mathbf{p}'_c = \mathbf{H}_0^{-1} \mathbf{K}^{-1} z_c \begin{bmatrix} u'_0 \\ v'_0 \\ 1 \end{bmatrix} \quad (2)$$

It is worth noticing that within the camera frame,  $\mathbf{p}'_c$  and  $\mathbf{p}_c$  share the same depth.  $\varphi'_0$  starts from the origin of the camera frame and ends at  $\mathbf{p}_c$ :

$$\varphi_0 = \mathbf{p}'_c - \mathbf{p}_c \quad (3)$$

$$\varphi'_0 = \mathbf{p}_c - \mathbf{o}_{c0} \quad (4)$$

where  $\mathbf{o}_{c0}$  is the coordinate of camera frame's origin in the robot base frame. Then we calculate the norm vector of  $S_0$ :  $\mathbf{n}_0 = \varphi_0 \times \varphi'_0$ . We can calculate  $\mathbf{n}_1$  in the same way. Finally, we generate the 3D post-contact vector in the robot base frame:  $\tau_c = \mathbf{n}_0 \times \mathbf{n}_1$ .

Finally, we use motion planning to conduct the one-step interaction with the articulated object. The motion planning process can be divided into two phases: we first let the hand move to the contact point and then we let the hand move a little distance in the direction of the post contact vector.

## B. Explicit World Model Construction

Building an explicit model of an articulated object is difficult because only if the geometries of all parts and kinematic relationships between connected parts are both figured out can the model of the articulated object be constructed.

In our work, we have two assumptions for the articulated objects: (1) the articulated object only contains a single prismatic or revolute joint; (2) the base link of the articulated object is fixed.

We choose Ditto [49] to construct the physical model explicitly. Given the visual observations before and after the interaction ( $\mathcal{P}_0$  and  $\mathcal{P}_1$ ), Ditto uses structured feature grids and unified implicit neural representation to construct part-level digital twins of articulated objects. Different from the original work where a multi-view fused point cloud is used, we use a single-view point cloud as input, which is more consistent with real robot application settings. Furthermore, we simulate the depth sensor's noise when generating training data to narrow the domain gap [50]. After we train the Ditto on simulated data, we use the trained model on the real two-frame point clouds to generate the implicit neural representation and extract the meshes. The explicit physics model is represented as the Unified Robot Description Format (URDF), which can be easily loaded into widely used multi-body physics simulators, such as SAPIEN [51].

The surface geometries of the real-world object are usually complex, thus the extracted meshes can be non-convex. We further perform convex decomposition using VHACD [52] before importing the meshes to the physics simulator, which is essential for realistic physics simulation of robot interaction.

### C. Sampling-based Model Predictive Control

Having an explicit physics model and a target joint state  $s_{target}$  of the articulated object, the agent needs to search for a trajectory that can change the current joint state  $s_{initial} = s_1$  to  $s_{target}$ . The expected relative joint movement is  $\Delta s_{target} = s_{target} - s_{initial}$ . Because of the complex contact between the robot end-effector and the constructed object model, the informative gradient of the objective function can hardly be acquired. Therefore, we employ sampling-based model predictive control, which is a zeroth-order method, to search for an optimal trajectory. There are various kinds of sampling-based model predictive control algorithms according to the zeroth-order optimization method used, such as Covariance Matrix Adaptation Evolution Strategy (CMA-ES) [53], Cross-Entropy Method (CEM) [54], and Model Predictive Path Integral Control (MPPI) [55]. Among these methods, we select the iCEM method [56] to search for a feasible long-horizon trajectory to complete the task due to its simplicity and effectiveness. We briefly describe how we apply the iCEM method in the following paragraph.

Trajectory length  $T \in \mathbb{N}^+$  denotes the maximum time steps in a trajectory. At each time step  $t (t < T)$ , the action of the robot  $\mathbf{a}_t \in \mathbb{R}^d$  is the incremental value of the joint position, where  $d$  is the number of degrees of freedom (DOF) of the robot. The population  $N$  denotes the number of samples sampled in each CEM iteration. Planning horizon  $h$  determines the number of time steps the robot plans in the future at each time step. The top  $K$  samples according to rewards compose an elite set, which is used to fit means and variances of a new Gaussian distribution. Please refer to [56] for details of the algorithm.

At each time step  $t$ , the agent generates an action for the robot  $\mathbf{a}_t \in \mathbb{R}^d$ , where  $d$  is the dimension of the action space. For 2-finger gripper tasks,  $d = 8$ , which consists of the 7 DOF of the robot arm and the 1 DOF of the gripper. However, for dexterous hands,  $d = 23$ , which includes the 7 DOF of the robot arm and the 16 DOF for the hand. The computational cost of iCEM is multiplied due to the high dimensionality of the action space. Consequently, directly searching in the original joint space of the multi-finger dexterous hand is not feasible. Moreover, the high-dimensional space of the dexterous hand may lead to unnatural postures. Therefore, it becomes essential to reduce the action space within the iCEM algorithm when using the dexterous hands.

In our work, we propose to use eigengrasp [9] to reduce the high-dimensional action space associated with dexterous hands. This approach involves clustering a substantial number of grasping object actions to extract low-dimensional principal components. These components are then linearly combined to approximate the hand's grasping posture. We first generate a dataset containing a diverse set of distinct grasping postures of the dexterous multi-finger hand in simulation using DexGraspNet [57]. We perform Principal Components Analysis (PCA) method on the dataset to get the largest  $m$  eigenvectors  $e_1, \dots, e_m$ . The iCEM algorithm is then performed on the action space  $\mathbf{a}_t \in \mathbb{R}^{7+m}$ . The joint angles of the hand  $\mathbf{q}_h$  are computed as a linear combination of the  $m$  eigenvectors:

$$\mathbf{q}_h = \sum_{i=1}^m (a_i \cdot e_i) \quad (5)$$

To speed up the search process, we use dense rewards to guide the trajectory optimization:

1) *Two-finger gripper*: For the two-finger gripper, the reward function consists of the following terms:

(1) *success reward*

$$r_{success} = \begin{cases} \omega_s, & \text{if } |s_{target} - s_t| < \epsilon \\ 0, & \text{else} \end{cases}$$

where  $s_t$  denotes the joint state at current time step  $t$ , and  $\epsilon$  is a predefined threshold.

(2) *approaching reward*

$$r_{target} = -\omega_t * (s_{target} - s_t) / (s_{target} - s_{initial})$$

This reward encourages  $s_t$  to converge to  $s_{target}$ .

(3) *contact reward*

$$r_{contact} = \begin{cases} \omega_{contact}, & \text{if } \frac{|s_t - s_{target}|}{|s_{target} - s_{initial}|} < 1 \\ -\omega_{collision}, & \text{if unexpected collision happens} \\ 0, & \text{else} \end{cases}$$

This reward encourages the robot to have first contact with the object in the correct direction and to keep in contact with the object when moving the part. Also, this reward tries to prevent parts other than the fingertip or the target part of the object from colliding.

(4) *distance reward*

$$r_{dist} = \omega_d * \|\mathbf{p}_{part} - \mathbf{p}_{grasp}\|^2$$

This reward encourages the gripper to get closer to the target part of the object, where  $\mathbf{p}_{part}, \mathbf{p}_{grasp} \in \mathbb{R}^3$  denotes the position of the geometry center of the target part and the grasp center of the gripper in Cartesian space, respectively.

(5) *regularization reward*

$$r_{reg} = - \sum_{i=0}^d (\omega_a * a_i + \omega_v * v_i)$$

This reward is a regularization reward that discourages the robot to move too fast or move to an unreasonable configuration.  $a_i$  and  $v_i$  denote the acceleration and velocity of the  $i$ th joint respectively.

2) *Dexterous hand*: For the dexterous hand, apart from the *success reward*  $r_{success}$  and *approaching reward*  $r_{target}$ , which remain consistent in the 2-finger gripper's reward function, the other three terms are as follows:

(1) *contact reward*

$$r_{contact} = \begin{cases} \omega_{contact}, & \text{if } \mathbf{ISCONTACT}(palm, obj) \text{ AND} \\ & \sum_{finger} \mathbf{ISCONTACT}(finger, obj) \geq 2 \\ 0, & \text{else} \end{cases}$$

This reward function encourages the dexterous hand to cage much of the target link while searching for the trajectory. With this reward, the dexterous hand can quickly find a stable

grasping position of the target link and keep in contact with the object while moving the part.

(2) *distance reward*

$$r_{dist} = \omega_d * \|\mathbf{p}_{part} - \mathbf{p}_{grasp}\|^2$$

This reward encourages the dexterous hand to get closer to the target part of the object, where  $\mathbf{p}_{part}, \mathbf{p}_{grasp} \in \mathbb{R}^3$  denotes the position of the geometry center of the target part and the grasp center of dexterous hand in Cartesian space, respectively.

(3) *regularization reward*

$$r_{reg} = - \sum_{i=0}^d (\omega_v * v_i + \omega_p * e_p)$$

This reward discourages the robot to move too fast by restricting the joints' velocity. The reward also discourages position error of the end link using cartesian error.  $v_i$  denotes the velocity of the  $i$ -th joint respectively and  $e_p$  denotes the cartesian error of the end effector.

Once the manipulation trajectory is generated, we execute the trajectory on the real robot.

#### IV. EXPERIMENTS

In this section, we evaluate the precision and effectiveness of the proposed method for manipulating articulated objects for both two-finger grippers and dexterous hands. We first conduct a large number of real-world articulated object manipulation experiments and quantitatively compare the performance. Then we design 4 ablation studies to verify the effectiveness of different modules of our method. Finally, we validate the operational advantage of the dexterous hand against the two-finger gripper by comparing the task execution efficiency in simulation.

##### A. Experimental Setup

Fig. 4 shows the real-world experimental setup. For the robot, a 7-DOF robot arm (ROKAE xMate3Pro) is used and an RGBD camera (Intel RealSense D415) is set to capture the visual input. The robot arm base is fixed at the table. Two kinds of end effectors are used: a 1-DoF 2-finger gripper (Robotiq 2F-140) and a 16-DoF 4-finger dexterous hand (Allegro Hand).

We choose 3 categories of common articulated objects for experiments, which are drawers, faucets and laptops as shown in Fig. 4(c). For the drawer, we assume that only one part of the drawer requires to be operated if there is more than one movable part. Besides, we only consider the case that the handle of the faucet rotates in horizontal direction. The articulated object is randomly located on the table with its base link fixed, and  $s_0$  is randomly set. We randomly select  $\Delta s_{target}$  which does not exceed the joint limit and covers both directions of possible movement.

To remove the influence of the background, we crop the object point cloud out of the scene using a bounding box. It is worth noting that we locate the camera on the right side of the robot rather than the front. This setting is better aligned with real application scenarios while increasing point cloud occlusion and manipulation difficulty. We further build

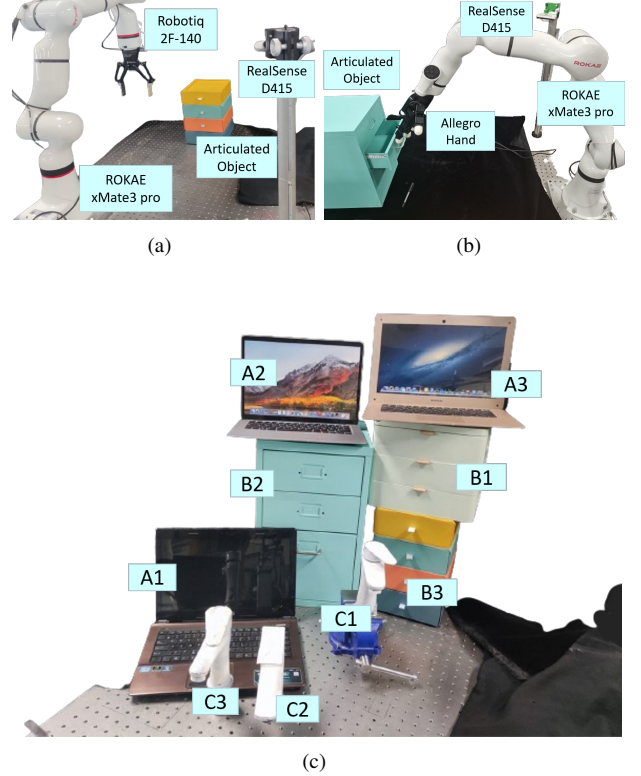


Fig. 4. (a) (b) Real-world experimental setup of two-finger gripper and dexterous hand. (c) Articulated object for manipulation. There are 3 categories of articulated objects in our real-world experiment.

the robot in simulation using the CAD models. We use SAPIEN [51] as the physics simulator to collect training data for the Explicit Physics Model Construction module and create simulation environments for the Sampling-based Model Predictive Control module.

##### B. Data Collection and Training

**Explicit Physics Model Construction.** For drawers and faucets, we choose 14 and 8 objects from Shape2Motion datasets [58]. For laptops, we choose 5 objects from PartNet-Mobility dataset [59] because the joint limits of laptops in PartNet-Mobility dataset are more reasonable than in Shape2Motion datasets. The original meshes are not watertight in the PartNet-Mobility dataset, which cannot be used to compute point occupancy, so we use ManifoldPlus [60] to fix the meshes. We reimplement the data collection code using SAPIEN simulator to keep consistency. When collecting data, the object is fixed on the origin and then randomly rotated around the z-axis by  $[-60^\circ, +60^\circ]$ . The camera is on a sphere centered on the object's center. Azimuth and Altitude of the camera are randomly sampled from  $[-60^\circ, +60^\circ]$  and  $[15^\circ, 45^\circ]$ . 10000 samples are collected for each category. We downsample the object point clouds to 8192 points. The 3 categories are trained jointly.

**Eigengrasp Dataset Construction.** To build the dataset for eigengrasp computation, we utilize DexGraspNet [57] to generate a collection of random grasping postures for the Allegro

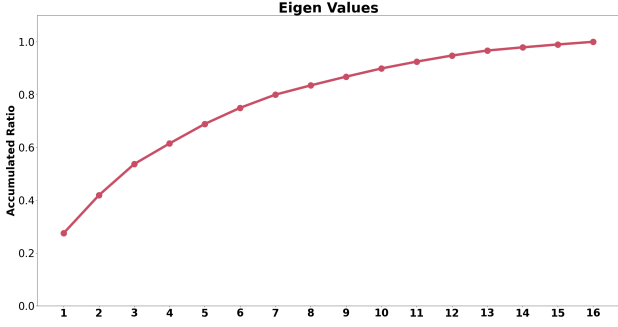


Fig. 5. Results of accumulated ratios of different eigengrasp dimensions.

Hand. The dataset includes 60800 grasp postures across 474 objects. We then compute the eigengrasp based on this data. Fig. 5 shows the accumulated ratios of different eigengrasp dimensions. Unless otherwise specified, we use eigengrasp dimension  $m = 2$  for dexterous manipulation experiments.

### C. Experiments on 2-Finger Gripper

1) *Real World Articulated Object Manipulation*: For parameters of the Interactive Perception module, we choose  $n_p = 10$  and  $n_a = 10$ . For parameters of the Sampling-based Model Predictive Control module, we find that  $T = 50$ ,  $N = 300$ ,  $h = 10$  and  $K = 20$  are able to complete all the tasks. The range of incremental value of joint position is set to  $[-0.05, 0.05]$ . The parameters in the reward function are determined manually according to experience in the simulation environment. We set  $\omega_s = 20$ ,  $\epsilon = 0.005$ (m or rad),  $\omega_t = 50$ ,  $\omega_{contact} = 10$ ,  $\omega_{collision} = 60$ ,  $\omega_d = 10$ ,  $\omega_a = 0.01$  and  $\omega_v = 0.03$ . We use 20 processes for sampling in simulation on a computer that has an Intel Core i7-12700 CPU and an NVIDIA 3080Ti GPU. It takes 4 minutes to find a feasible trajectory.

We conduct about 30 experiments for each category. After the trajectory is executed in the real world, we measure the real joint movement  $\Delta s_{real} = s_{real} - s_{initial}$  and compare it with the target joint movement  $\Delta s_{target} = s_{target} - s_{initial}$ . We compute the error  $\delta = \Delta s_{real} - \Delta s_{target}$  and the relative error  $\delta_r = \delta / \Delta s_{target} \times 100\%$ , results of all the experiments can be found in Fig. 6, and statistical results can be found in Table I. Trajectories of both opening and closing the laptop are shown in Fig. 7.

Among all 3 categories, the drawer has the lowest  $|\delta_r|$  and the faucet has the highest  $|\delta_r|$  according to Table I. It is reasonable because the size of the faucet is relatively small, a minor inaccuracy in model construction or trajectory execution will result in a big error in the joint state. About 70% of manipulations achieve a  $|\delta_r| < 30\%$  for drawers and laptops, which shows the accuracy of our method.

Errors may be caused by the following factors:

- (1) The constructed mesh is not accurate enough, especially for the parts that are occluded. For example, the inside face of the drawer front cannot be observed by the RGBD camera, so when the digital twin is constructed, the drawer front is thicker than the real one. It causes the

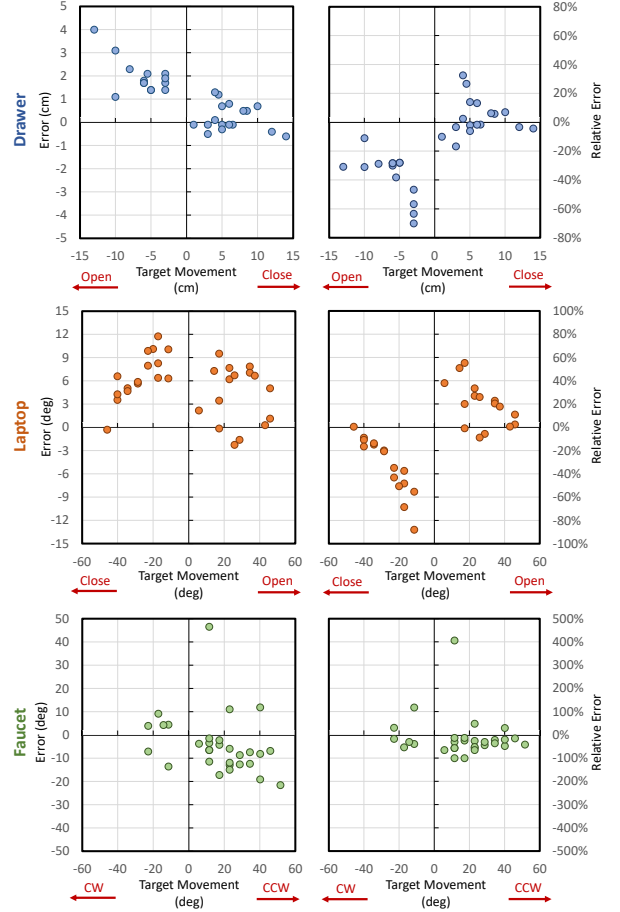


Fig. 6. Experimental results of real-world articulated object manipulation with 2-finger gripper. Each row refers to the results of one category. The left column shows the error  $\delta$  of the manipulation. The right column shows the relative error  $\delta_r$  of the manipulation. The sign of the target movement denotes the direction of the movement (e.g. opening or closing, clockwise (CW) or counterclockwise (CCW)).

TABLE I  
ACCURACY OF REAL ARTICULATED OBJECTS MANIPULATION WITH 2-FINGER GRIPPER

Category		Drawer	Laptop	Faucet
Number of manipulations		31	32	30
Number of manipulations s.t. $ \delta_r $	$<10\%$	12	7	0
	$<30\%$	22	20	9
	$<50\%$	28	26	19
Avg $ \delta $		1.15cm	5.69°	10.37°
Avg $ \delta_r $		21.81%	27.26%	56.21%

results of opening tasks of drawers (which has average  $|\delta|$  of 2cm) to be worse than closing tasks (which have average  $|\delta|$  of 0.5cm). It is worth noting that there is a relative error of over 400% in turning faucet tasks. This happens because the robot touches the part close to the joint axis first (which does not occur in the simulation), causing a huge rotation of the handle.

- (2) The dynamic properties of the real articulated objects are complicated. For example, the elastic deformation of laptops is not modeled in the simulation.
- (3) The kinematic structure of a real articulated object is not



ideal. For example, there might be gaps in the drawer rails, which turns the original prismatic joint into a joint with several DOFs.

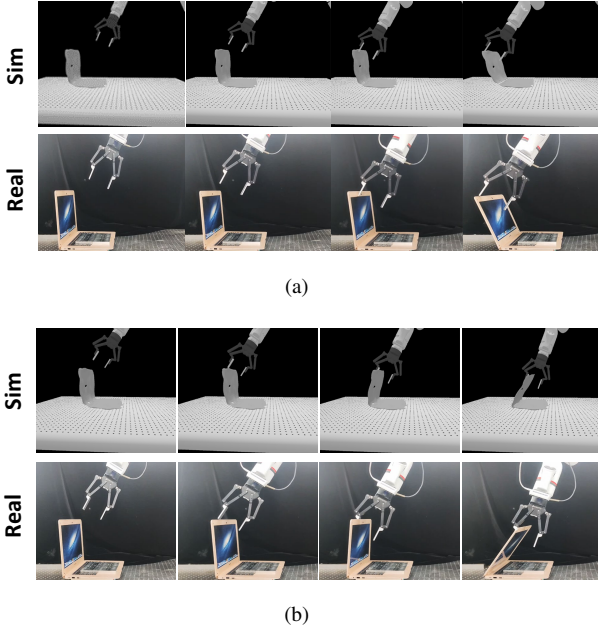


Fig. 7. Trajectories of laptop manipulation with 2-finger gripper: (a) open; (b) close. The constructed digital twin precisely captures the kinematic property of the articulated object, leading to the accurate alignment of Sim and Real.

2) *Ablation Study on Reward Function*: The reward function in the sampling-based model predictive control module is designed to guide the robot to complete the task. To examine the impact of each term of the reward function, we conduct the ablation study. There are 5 terms in the reward function, so 6 groups of experiments are conducted to reveal each term’s influence against the full reward function. The first group runs iCEM with the full reward function as in Section III-C. Each of the other 5 groups drops one term of the full reward function. In each group, 5 tasks are conducted to make the results more general. The task that is considered to be failed if not completed within 50 time steps. Fig. 8 summarizes the experimental results.

The experiments using the full reward function are superior in both success rate and steps to succeed, except for the experiments without  $r_{reg}$ . However, the trajectories searched in w/o  $r_{reg}$  are not suitable for real-world execution, because the robot tends to move to an unusual configuration which could be dangerous. Without  $r_{dist}$ , the robot cannot complete the task because the horizon is too short to achieve a positive reward. Omitting  $r_{target}$ ,  $r_{success}$ , or  $r_{contact}$  results in lower success rates, and even when successful, the robot requires more steps to complete the task.

#### D. Experiments on Dexterous Hand

1) *Real World Articulated Object Manipulation*: For each 3 categories, we choose one object for real object manipulation experiments. Considering the FOV of the RGBD camera as well as the workspace of motion planning, we randomly set the

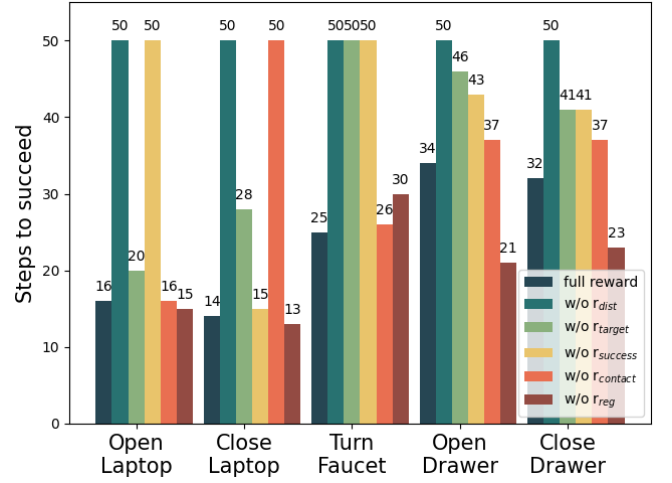


Fig. 8. Results of ablation study on reward function. The 5 tasks are opening/closing drawer, opening/closing laptop and turning faucet. The task is considered to be failed if it is not done when time step reaches 50.

location and initial joint status  $s_0$  of articulated objects on the table in a certain range, such that the object is in the workspace of the manipulator. We randomly select  $\Delta s_{target}$  which does not exceed the joint limit and covers both directions of possible movement.

For each category, we conduct 30 experiments. For parameters of Sampling-based Model Predictive Control module, we find that  $T = 50$ ,  $N = 100$ ,  $h = 10$  leads to fast searching as well as good performance. For the parameters in the reward function, we make adjustments based on the results of simulation experiments. We set  $\omega_s = 20$ ,  $\omega_t = 50$ ,  $\omega_{contact} = 10$ ,  $\omega_d = 10$ ,  $\omega_c = 0.001$  and  $\omega_v = 0.01$ . We use eigen dimension  $m = 2$  to conduct real world manipulation. We use 10 processes for sampling in simulation on a computer that has an Intel Core i7-12700 CPU and an NVIDIA 3080Ti GPU. It takes about 2.5 minutes to find a feasible trajectory.

Results of all the experiments can be found in Fig. 9, and statistical results can be found in Table II. Trajectories of opening and closing a drawer are shown in Fig. 10. Similar to manipulation with 2-finger gripper, the drawer has the lowest  $|\delta_r|$  and the faucet has the highest  $|\delta_r|$  according to Table II.

TABLE II  
ACCURACY OF REAL ARTICULATED OBJECTS MANIPULATION WITH DEXTEROUS HAND

Category	Drawer	Laptop	Faucet	
Number of manipulations	32	31	26	
Number of manipulations s.t. $ \delta_r $	<20%	14	12	4
	<40%	22	23	18
	<60%	27	27	22
Avg $ \delta $	1.90cm	6.92°	9.48°	
Avg $ \delta_r $	28.25%	30.76%	45.72%	

2) *Ablation Studies*: For the ablation study of dexterous hand manipulation, we investigate the impact of several key factors. Specifically, we analyze the influences of eigen-grasp dimensions on Sampling-based Model Predictive Control, study how pixel projection affects the Interactive Perception

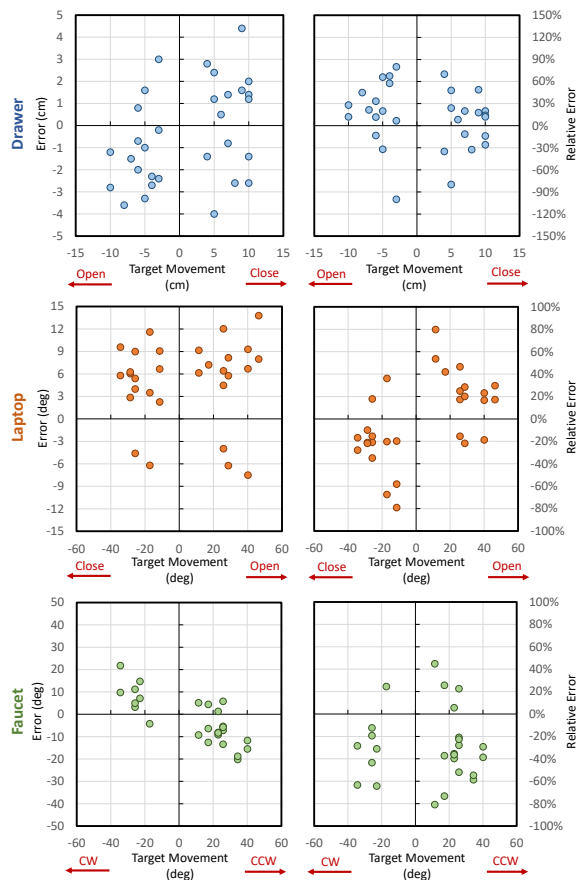


Fig. 9. Experiment results of real-world articulated object manipulation with dexterous hands. Each row refers to the results of one category. The left column shows the error  $\delta$  of the manipulation. The right column shows the relative error  $\delta_r$  of the manipulation. The sign of the target movement denotes the direction of the movement (e.g. opening or closing, clockwise (CW) or counterclockwise (CCW)).

module and also explore the influences of different reward functions.

**Eigengrasp Dimension.** In Section III-C2, we propose to utilize eigengrasp to reduce the dimension of action space, enhancing the efficiency of our search process. To evaluate the effectiveness of MPC with different eigengrasp dimensions, we conduct experiments with dimensions  $m = 1, 2, 7, 16$ . We adopt 3 performance metrics: success rate, joint jerk, and computation time. We evaluate on 5 different tasks in simulation: opening/closing laptop, turning faucet, and opening/closing drawer. Each task is repeated 10 times with randomized object positions and initial robot configurations.

- 1) **Success rate** Fig.11 presents the success rate of each task with different dimensions. The tasks of opening laptop and closing drawer achieve a 100% success across all the 4 dimension numbers. This high success rate likely stems from the simplicity of these tasks. However, in the tasks of closing the laptop and opening the drawer, trajectories generated with  $m = 1$  shows a significantly lower success rate compared to the other dimensions.

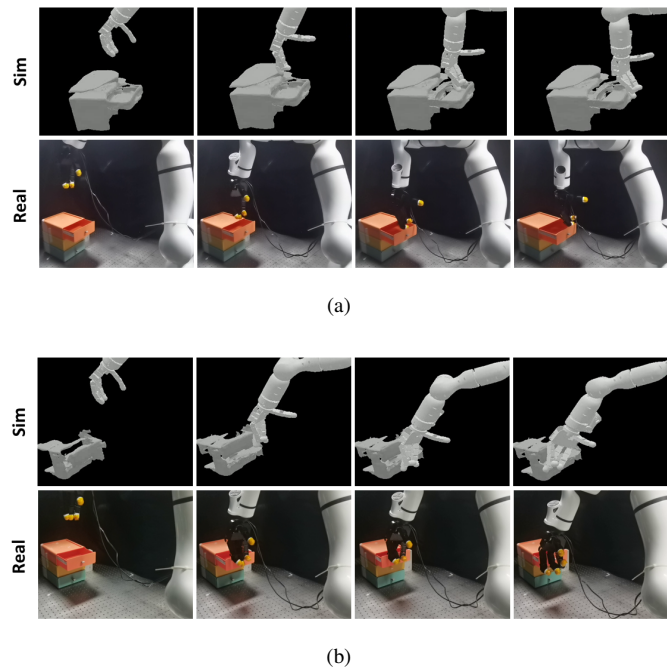


Fig. 10. Trajectories of drawer manipulation with dexterous hand: (a) open; (b) close. The constructed digital twin precisely captures the kinematic property of the articulated object, leading to the accurate alignment of Sim and Real.

This may be attributed to the reduced dexterity of the Allegro Hand when operating in a 1-DOF configuration. Interestingly, for all the 5 tasks, the dimension reduced to  $m = 2$  performs comparably to  $m = 7, 16$ . This finding highlights the effectiveness of using eigengrasp space with  $m = 2$ , achieving similar success rates while reducing computation time.

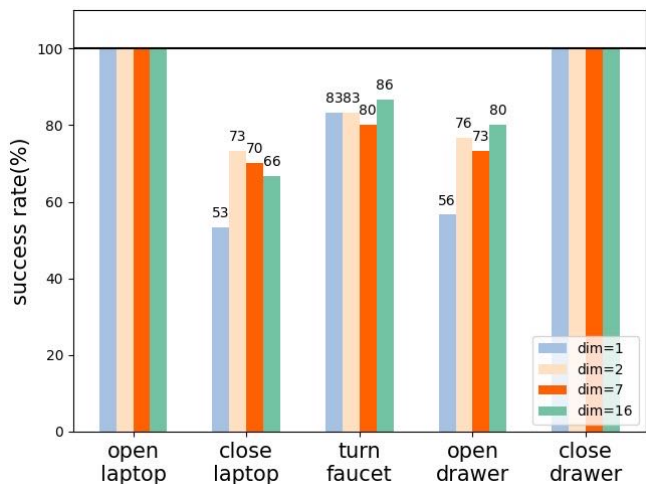


Fig. 11. Success rate with different eigengrasp dimensions.

- 2) **Joint jerk** For real robot control, joint jerk reflects the smoothness of a robot's movements. Our study investigates how the eigengrasp dimension affects the jerks of dexterous hand joints. To quantify jerk, we utilize the third derivative of hand joint positions with respect to time. Specifically, we calculate the average jerk for each

finger at every time step, reflecting the smoothness of finger movement. Fig 12 illustrates the results for the 5 tasks. Our experimental results consistently demonstrate that finger joint jerks increase with higher eigengrasp dimensions. Remarkably, for all the 5 tasks, dimension  $m = 1$  exhibits superior performance in terms of thumb jerk compared to  $m = 2, 7, 16$ . However, for the remaining three fingers: both  $m = 1, 2$  demonstrate similar advantages over higher dimensions.

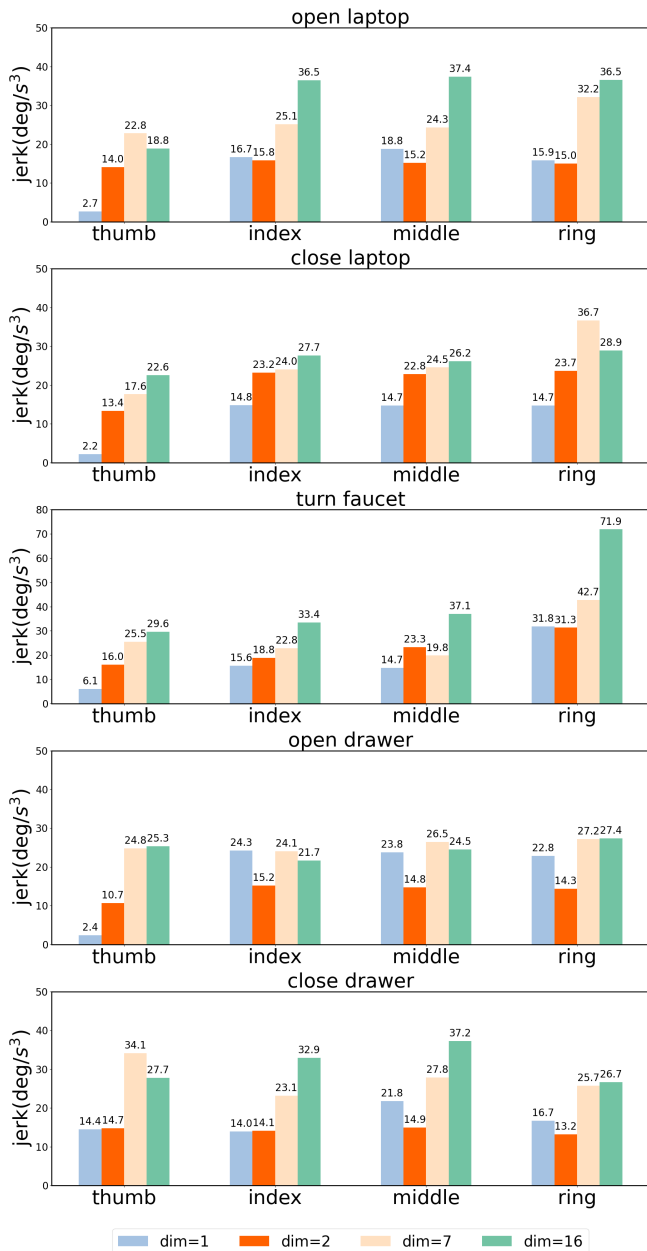


Fig. 12. Joint jerk with different eigengrasp dimensions.

- 3) **Computation time** For each task, we generate 30 different trajectories and compare the average time per step as shown in Fig 13. It is shown that using eigengrasp dimension  $m = 2$  results in approximately 1 second less per step compared to 16 dimensions. Consequently, it takes nearly 1 minute less to find a feasible trajectory.

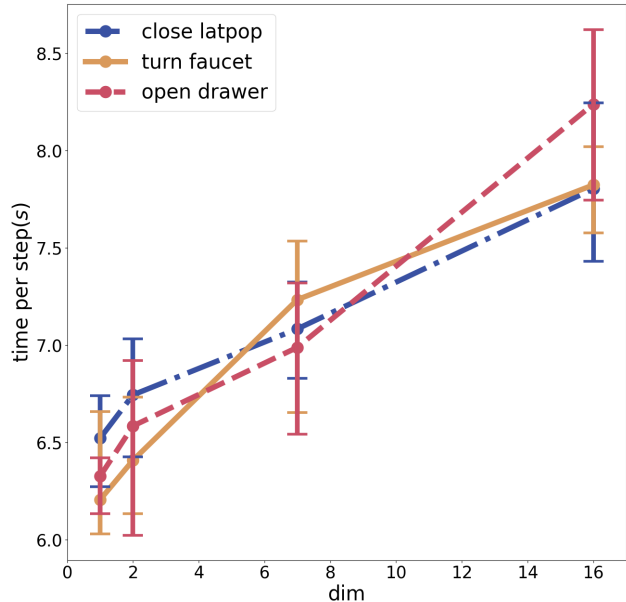


Fig. 13. Computation time with different eigengrasp dimensions.

**Pixel Projection.** In Section III-A2, we propose a pixel projection method that leverages both RGB images and depth information of an object to transform a 2D post-contact vector into a 3D robot trajectory. To evaluate the necessity of the pixel projection approach, we compare it with randomly generated vectors based solely on 2D affordance. Specifically, we select one object per category and generate three random vectors for each object. The results, shown in Fig. 14, demonstrate that the vector synthesized by pixel transformation is better suited for executing one-step interactions compared to the randomly generated direction vector.

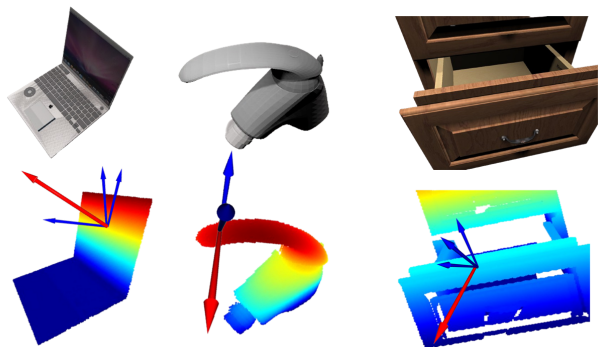


Fig. 14. Ablation study on pixel projection. The red vector represents the vector generated by using pixel projection. The three blue vectors are generated only based on 2D affordance.

**Reward Function.** In Section III-C2, we design reward function in the sampling-based model predictive control module for dexterous hand manipulation tasks. Five terms of reward functions are designed, which include  $r_{success}$ ,  $r_{target}$ ,  $r_{contact}$ ,  $r_{dist}$  and  $r_{reg}$ . We conduct 5 groups of experiments to reveal each term's influence against the full reward function. The first

group runs iCEM with the full reward function as in III-C. The other 4 experiments drop one term of the full reward function. To make the ablation result more generalizable, we conduct 3 tasks for each group: opening laptop, closing laptop and turning faucet. In each task, we randomize the position of the object, the initial joint angle of the robot as well as the target qpos of the object to generate 30 different trajectory running iCEM. The task that is not done when time step reaches 50 is considered failed. Fig. 15(a) and Fig. 15(b) respectively summarize the experimental results.

The experiments using the full reward function consistently outperforms others in terms of both success rate and steps in completion, except for the experiments without  $r_{contact}$ . It’s worth noticing that the reward function without  $r_{contact}$  even exhibits a surprising advantage in terms of the number of steps to success in task 2. This unexpected result may be attributed to the absence of constraints imposed by the human-like hand posture encouraged by  $r_{contact}$ . Without this component, the iCEM algorithm might explore unconventional hand postures to interact with the object. On the other hand, omitting  $r_{dist}$  from the reward function makes the tasks impossible to accomplish for the robot. The short planning horizon prevents the robot from accumulating positive rewards. Similarly, excluding  $r_{target}$  and  $r_{success}$  leads to decreased success rates. In successful cases, the robot requires additional steps to accomplish the task.

3) *Advantage of Dexterous Manipulation*: In this section, we validate the advantages of the dexterous hand over the two-finger gripper through experiments on five tasks. For each task, we randomize the object’s position and the robot’s initial configuration 10 times. We then run the iCEM algorithm using both the Allegro hand and the Robotiq gripper. We use the number of steps to complete the task as the metrics.

Fig. 16 summarizes the comparison results between the dexterous hand and the two-finger gripper. Except for the laptop opening task, the dexterous hand consistently requires fewer steps on average. The anomaly in the laptop opening task can be attributed to its simplicity, as it does not require precise contact between the end effector and the object. Fig. 17 visualizes the trajectories for the laptop closing task, showing that our method is able to find a shorter trajectory for the dexterous hand by utilizing its additional degrees of freedom to close the laptop efficiently.

### E. Effectiveness of Interactive Perception

The Interactive Perception module is designed to improve the accuracy of the constructed world model by utilizing the two different point clouds captured before and after interaction. To evaluate its necessity, we train another model using a single-frame point cloud as the network input. For each category of objects, we select one real object and compare the modeling results of two-frame and single-frame point cloud inputs. Fig. 18 shows the comparison results. The findings demonstrate that actively interacting with the movable part of the object and altering its state allows us to build a transition model with more accurate segmentation of movable parts and joint axis estimation, which is necessary for precise manipulation.

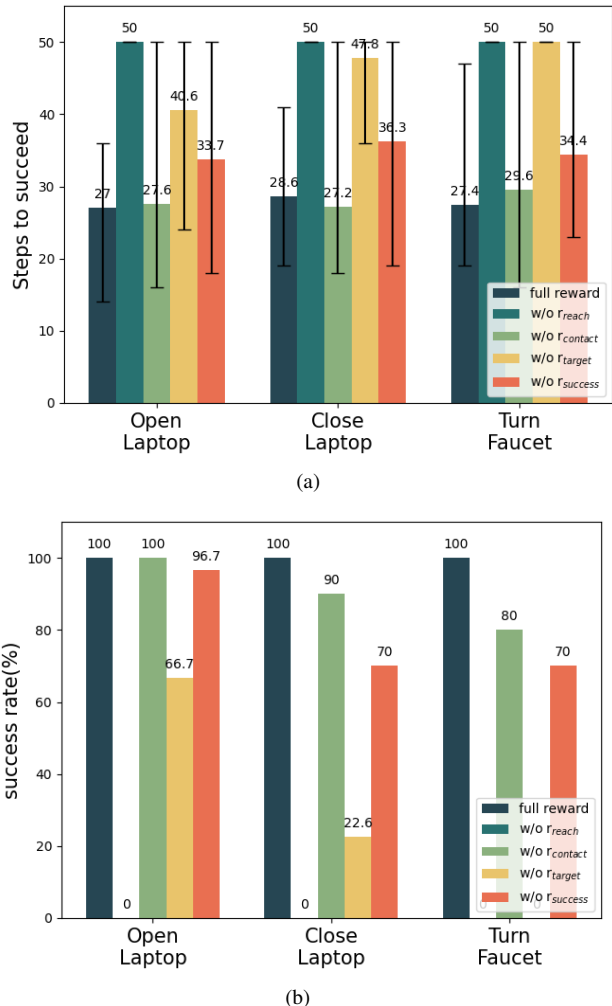


Fig. 15. Results of numbers of steps to succeed (a) and results of success rate (b). The task is considered to be failed if it is not done when time step reaches 50.

### F. Advanced Manipulation Skills

By utilizing a physics simulation as the explicit world model, our method ensures generalizability to unseen actions. This allows for easy extension to advanced manipulation skills, such as manipulation with tools. As shown in Fig. 19, when the drawer is located out of the dexterous range of the robot or the gap between the drawer front and body is too small, the gripper alone cannot open it. In such cases, the robot can employ nearby tools to complete the task.

To demonstrate our method’s tool-using capability, we use two different tools for the drawer-opening task. Benefiting from the explicit physics model, we can equip the robot with a tool to interact with the articulated object in the simulation. When using MPC to search for trajectories, we assume the tool is mounted on the robot’s end effector. We simply replace the gripper tips with the tool in  $r_{dist}$  when computing rewards. Remarkably, our method successfully finds a feasible trajectory with most parameters unchanged.

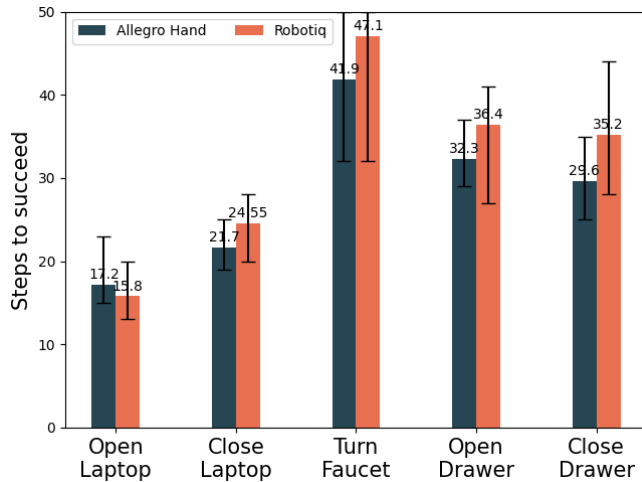


Fig. 16. Comparison of manipulation with dexterous hand and two-finger gripper.

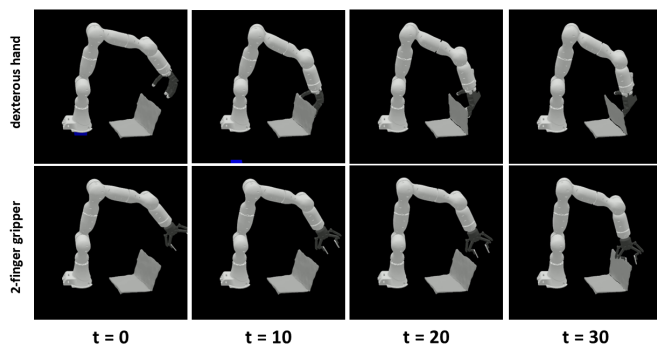


Fig. 17. Trajectory comparison of a dexterous hand and a 2-finger gripper performing the same laptop-closing task. The dexterous hand completes the task in fewer steps.

## V. CONCLUSION AND DISCUSSION

In this work, we present DexSim2Real<sup>2</sup>, a novel robot learning framework designed for precise, goal-conditioned articulated object manipulation with two-finger grippers and dexterous hands. We first build the explicit world model of the target object in a physics simulator through active interaction and then use MPC to search for a long-horizon manipulation trajectory to achieve the desired manipulation goal. Quantitative evaluation of real object manipulation results verifies the effectiveness of our proposed framework for both kinds of end effectors.

For future work, we plan to integrate proprioceptive sensing and tactile sensing during real-robot interaction to refine the constructed world model for more precise manipulation. 3D generative AI has seen great progress in the last few years. We also plan to integrate the AIGC technique to improve the geometry quality of the digital twin. Besides, a module that estimates the state of the object in real time will enhance reactive manipulations. Lastly, we aim to expand the framework to include mobile manipulation, objects with multiple movable parts and deformable objects, thereby broadening its applicability across various robotic tasks.

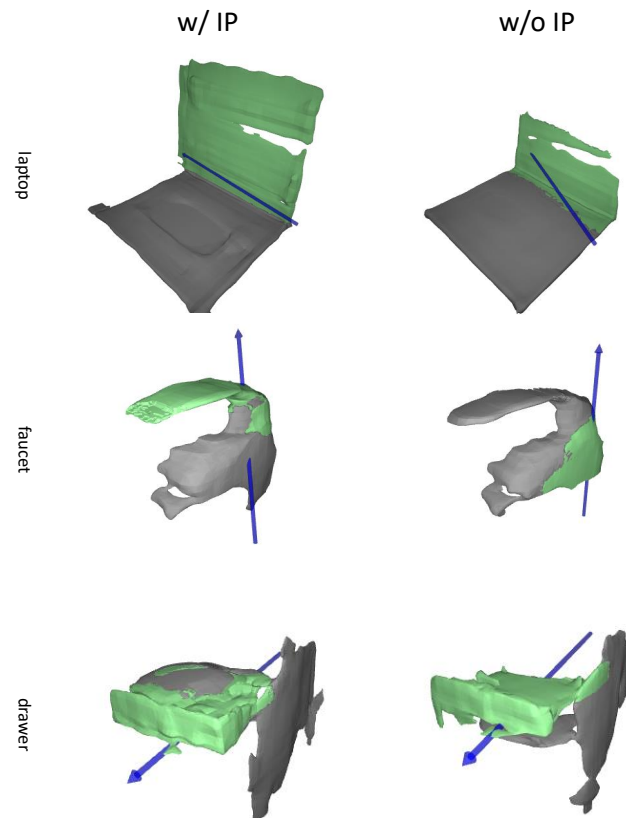


Fig. 18. Ablation study on Interactive Perception. The model constructed with Interactive Perception has more accurate movable part segmentation and joint axis estimation.

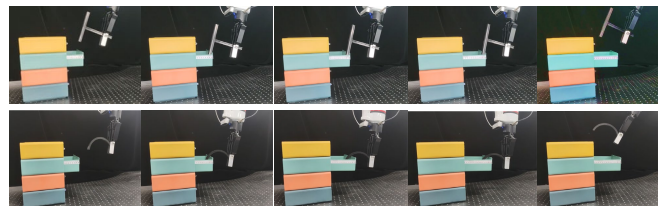


Fig. 19. Open drawer with tools. In real scenarios, the object may be beyond the robot’s reach, or the gripper cannot fit into the object’s size. Our method can be extended to tool-using cases. As shown in these two sequences, the robot uses a T-shaped tool or a semi-ring to open the small drawer.

## REFERENCES

- [1] Z. Xu, Z. He, and S. Song, “Universal manipulation policy network for articulated objects,” *IEEE Robotics and Automation Letters*, vol. 7, no. 2, pp. 2447–2454, 2022.
- [2] P. Xie, R. Chen, S. Chen, Y. Qin, F. Xiang, T. Sun, J. Xu, G. Wang, and H. Su, “Part-guided 3d rl for sim2real articulated object manipulation,” *IEEE Robotics and Automation Letters*, 2023.
- [3] Y. Wang, R. Wu, K. Mo, J. Ke, Q. Fan, L. J. Guibas, and H. Dong, “Adaafford: Learning to adapt manipulation affordance for 3d articulated objects via few-shot interactions,” in *European conference on computer vision*. Springer, 2022, pp. 90–107.
- [4] T. Mu, Z. Ling, F. Xiang, D. C. Yang, X. Li, S. Tao, Z. Huang, Z. Jia, and H. Su, “Maniskill: Generalizable manipulation skill benchmark with large-scale demonstrations,” in *Thirty-fifth Conference on Neural Information Processing Systems Datasets and Benchmarks Track (Round 2)*, 2021.

- [5] J. Gu, F. Xiang, X. Li, Z. Ling, X. Liu, T. Mu, Y. Tang, S. Tao, X. Wei, Y. Yao *et al.*, “Maniskill2: A unified benchmark for generalizable manipulation skills,” in *The Eleventh International Conference on Learning Representations*, 2023.
- [6] S. H. Johnson, “Thinking ahead: the case for motor imagery in prospective judgements of prehension,” *Cognition*, vol. 74, no. 1, pp. 33–70, 2000.
- [7] C. Von Hofsten, “Action in development,” *Developmental science*, vol. 10, no. 1, pp. 54–60, 2007.
- [8] C. V. Hofsten, “Action, the foundation for cognitive development,” *Scandinavian Journal of Psychology*, vol. 50, no. 6, pp. 617–623, 2009.
- [9] M. Ciocarlie, C. Goldfeder, and P. Allen, “Dexterous grasping via eigen-grasps: A low-dimensional approach to a high-complexity problem,” in *Robotics: Science and systems manipulation workshop-sensing and adapting to the real world*, 2007.
- [10] M. Kiatos, S. Malassiotis, and I. Sarantopoulos, “A geometric approach for grasping unknown objects with multifingered hands,” *IEEE Transactions on Robotics*, vol. 37, no. 3, pp. 735–746, 2021.
- [11] T. Pang, H. J. T. Suh, L. Yang, and R. Tedrake, “Global planning for contact-rich manipulation via local smoothing of quasi-dynamic contact models,” *IEEE Transactions on Robotics*, vol. 39, no. 6, pp. 4691–4711, 2023.
- [12] A. Agarwal, S. Uppal, K. Shaw, and D. Pathak, “Dexterous functional grasping,” in *7th Annual Conference on Robot Learning*, 2023.
- [13] L. Ma, J. Meng, S. Liu, W. Chen, J. Xu, and R. Chen, “Sim2real2: Actively building explicit physics model for precise articulated object manipulation,” in *2023 IEEE International Conference on Robotics and Automation (ICRA)*, 2023, pp. 11 698–11 704.
- [14] A. Okamura, N. Smaby, and M. Cutkosky, “An overview of dexterous manipulation,” in *Proceedings 2000 ICRA. Millennium Conference. IEEE International Conference on Robotics and Automation. Symposia Proceedings (Cat. No.00CH37065)*, vol. 1, 2000, pp. 255–262 vol.1.
- [15] D. Rus, “In-hand dexterous manipulation of piecewise-smooth 3-d objects,” *The International Journal of Robotics Research*, vol. 18, no. 4, pp. 355–381, 1999.
- [16] M. R. Dogar and S. S. Srinivasa, “Push-grasping with dexterous hands: Mechanics and a method,” in *2010 IEEE/RSJ International Conference on Intelligent Robots and Systems*. IEEE, 2010, pp. 2123–2130.
- [17] V. Kumar, E. Todorov, and S. Levine, “Optimal control with learned local models: Application to dexterous manipulation,” in *2016 IEEE International Conference on Robotics and Automation (ICRA)*. IEEE, 2016, pp. 378–383.
- [18] A. Wu, M. Guo, and C. K. Liu, “Learning diverse and physically feasible dexterous grasps with generative model and bilevel optimization,” *arXiv preprint arXiv:2207.00195*, 2022.
- [19] A. Gupta, C. Eppner, S. Levine, and P. Abbeel, “Learning dexterous manipulation for a soft robotic hand from human demonstrations,” in *2016 IEEE/RSJ International Conference on Intelligent Robots and Systems (IROS)*. IEEE, 2016, pp. 3786–3793.
- [20] I. Radosavovic, X. Wang, L. Pinto, and J. Malik, “State-only imitation learning for dexterous manipulation,” in *2021 IEEE/RSJ International Conference on Intelligent Robots and Systems (IROS)*. IEEE, 2021, pp. 7865–7871.
- [21] Y. Qin, H. Su, and X. Wang, “From one hand to multiple hands: Imitation learning for dexterous manipulation from single-camera teleoperation,” *IEEE Robotics and Automation Letters*, vol. 7, no. 4, pp. 10 873–10 881, 2022.
- [22] O. M. Andrychowicz, B. Baker, M. Chociej, R. Jozefowicz, B. McGrew, J. Pachocki, A. Petron, M. Plappert, G. Powell, A. Ray *et al.*, “Learning dexterous in-hand manipulation,” *The International Journal of Robotics Research*, vol. 39, no. 1, pp. 3–20, 2020.
- [23] Y. Qin, B. Huang, Z.-H. Yin, H. Su, and X. Wang, “Dexpoint: Generalizable point cloud reinforcement learning for sim-to-real dexterous manipulation,” in *Proceedings of The 6th Conference on Robot Learning*, ser. Proceedings of Machine Learning Research, K. Liu, D. Kulic, and J. Ichnowski, Eds., vol. 205. PMLR, 14–18 Dec 2023, pp. 594–605. [Online]. Available: <https://proceedings.mlr.press/v205/qin23a.html>
- [24] T. Chen, J. Xu, and P. Agrawal, “A system for general in-hand object re-orientation,” in *Conference on Robot Learning*. PMLR, 2022, pp. 297–307.
- [25] M. S. Branicky, V. S. Borkar, and S. K. Mitter, “A unified framework for hybrid control: Model and optimal control theory,” *IEEE transactions on automatic control*, vol. 43, no. 1, pp. 31–45, 1998.
- [26] R. S. Sutton, “Dyna, an integrated architecture for learning, planning, and reacting,” *ACM Sigart Bulletin*, vol. 2, no. 4, pp. 160–163, 1991.
- [27] A. Achille and S. Soatto, “A separation principle for control in the age of deep learning,” *Annual Review of Control, Robotics, and Autonomous Systems*, vol. 1, no. 1, pp. 287–307, 2018.
- [28] P. S. Castro, “Scalable methods for computing state similarity in deterministic markov decision processes,” in *Proceedings of the AAAI Conference on Artificial Intelligence*, vol. 34, no. 06, 2020, pp. 10 069–10 076.
- [29] N. A. Hansen, H. Su, and X. Wang, “Temporal difference learning for model predictive control,” in *International Conference on Machine Learning*. PMLR, 2022, pp. 8387–8406.
- [30] C. Finn, I. Goodfellow, and S. Levine, “Unsupervised learning for physical interaction through video prediction,” *Advances in neural information processing systems*, vol. 29, 2016.
- [31] C. Finn and S. Levine, “Deep visual foresight for planning robot motion,” in *2017 IEEE International Conference on Robotics and Automation (ICRA)*. IEEE, 2017, pp. 2786–2793.
- [32] P. Wu, A. Escontrela, D. Hafner, P. Abbeel, and K. Goldberg, “Daydreamer: World models for physical robot learning,” in *Conference on robot learning*. PMLR, 2023, pp. 2226–2240.
- [33] S. Yang, Y. Du, S. K. S. Ghasemipour, J. Tompson, L. P. Kaelbling, D. Schuurmans, and P. Abbeel, “Learning interactive real-world simulators,” in *The Twelfth International Conference on Learning Representations*.
- [34] S. Deng, X. Xu, C. Wu, K. Chen, and K. Jia, “3d affordancenet: A benchmark for visual object affordance understanding,” in *Proceedings of the IEEE/CVF Conference on Computer Vision and Pattern Recognition (CVPR)*, June 2021, pp. 1778–1787.
- [35] L. Cui, X. Chen, H. Zhao, G. Zhou, and Y. Zhu, “Strap: Structured object affordance segmentation with point supervision,” *arXiv preprint arXiv:2304.08492*, 2023.
- [36] K. Mo, L. J. Guibas, M. Mukadam, A. Gupta, and S. Tulsiani, “Where2act: From pixels to actions for articulated 3d objects,” in *Proceedings of the IEEE/CVF International Conference on Computer Vision*, 2021, pp. 6813–6823.
- [37] M. Deitke, D. Schwenk, J. Salvador, L. Weihs, O. Michel, E. VanderBilt, L. Schmidt, K. Ehsani, A. Kembhavi, and A. Farhadi, “Objaverse: A universe of annotated 3d objects,” in *Proceedings of the IEEE/CVF Conference on Computer Vision and Pattern Recognition*, 2023, pp. 13 142–13 153.
- [38] M. Deitke, R. Liu, M. Wallingford, H. Ngo, O. Michel, A. Kusupati, A. Fan, C. Laforte, V. Voleti, S. Y. Gadre *et al.*, “Objaverse-xl: A universe of 10m+ 3d objects,” *Advances in Neural Information Processing Systems*, vol. 36, 2024.
- [39] T. Nagarajan, C. Feichtenhofer, and K. Grauman, “Grounded human-object interaction hotspots from video,” in *Proceedings of the IEEE/CVF International Conference on Computer Vision*, 2019, pp. 8688–8697.
- [40] S. Bahl, R. Mendonca, L. Chen, U. Jain, and D. Pathak, “Affordances from human videos as a versatile representation for robotics,” 2023.
- [41] H. Bharadhwaj, R. Mottaghi, A. Gupta, and S. Tulsiani, “Track2act: Predicting point tracks from internet videos enables diverse zero-shot robot manipulation,” *arXiv preprint arXiv:2405.01527*, 2024.
- [42] S. James, Z. Ma, D. R. Arrojo, and A. J. Davison, “Rlbench: The robot learning benchmark & learning environment,” *IEEE Robotics and Automation Letters*, vol. 5, no. 2, pp. 3019–3026, 2020.
- [43] Y. Zhu, J. Wong, A. Mandlekar, and R. Martín-Martín, “robosuite: A modular simulation framework and benchmark for robot learning,” *arXiv preprint arXiv:2009.12293*, 2020.
- [44] V. Makoviychuk, L. Wawrzyniak, Y. Guo, M. Lu, K. Storey, M. Macklin, D. Hoeller, N. Rudin, A. Allshire, A. Handa *et al.*, “Isaac gym: High performance gpu-based physics simulation for robot learning,” *arXiv preprint arXiv:2108.10470*, 2021.
- [45] W. Chen, J. Xu, F. Xiang, X. Yuan, H. Su, and R. Chen, “General-purpose sim2real protocol for learning contact-rich manipulation with marker-based visuo-tactile sensors,” *IEEE Transactions on Robotics*, vol. 40, pp. 1509–1526, 2024.
- [46] F. Sadeghi, A. Toshev, E. Jang, and S. Levine, “Sim2real viewpoint invariant visual servoing by recurrent control,” in *Proceedings of the IEEE Conference on Computer Vision and Pattern Recognition*, 2018, pp. 4691–4699.
- [47] S. Höfer, K. Bekris, A. Handa, J. C. Gamboa, M. Mozifian, F. Golemo, C. Atkeson, D. Fox, K. Goldberg, J. Leonard *et al.*, “Sim2real in robotics and automation: Applications and challenges,” *IEEE transactions on automation science and engineering*, vol. 18, no. 2, pp. 398–400, 2021.
- [48] K. Dimitropoulos, I. Hatzilygeroudis, and K. Chatzilygeroudis, “A brief survey of sim2real methods for robot learning,” in *International Conference on Robotics in Alpe-Adria Danube Region*. Springer, 2022, pp. 133–140.

- [49] Z. Jiang, C.-C. Hsu, and Y. Zhu, "Ditto: Building digital twins of articulated objects from interaction," in *arXiv preprint arXiv:2202.08227*, 2022.
- [50] X. Zhang, R. Chen, F. Xiang, Y. Qin, J. Gu, Z. Ling, M. Liu, P. Zeng, S. Han, Z. Huang *et al.*, "Close the visual domain gap by physics-grounded active stereovision depth sensor simulation," *arXiv preprint arXiv:2201.11924*, 2022.
- [51] F. Xiang, Y. Qin, K. Mo, Y. Xia, H. Zhu, F. Liu, M. Liu, H. Jiang, Y. Yuan, H. Wang, L. Yi, A. X. Chang, L. J. Guibas, and H. Su, "SAPIEN: A simulated part-based interactive environment," in *The IEEE Conference on Computer Vision and Pattern Recognition (CVPR)*, June 2020.
- [52] K. Mamou and F. Ghorbel, "A simple and efficient approach for 3d mesh approximate convex decomposition," in *2009 16th IEEE international conference on image processing (ICIP)*. IEEE, 2009, pp. 3501–3504.
- [53] N. Hansen, S. D. Müller, and P. Koumoutsakos, "Reducing the time complexity of the derandomized evolution strategy with covariance matrix adaptation (cma-es)," *Evolutionary computation*, vol. 11, no. 1, pp. 1–18, 2003.
- [54] Z. I. Botev, D. P. Kroese, R. Y. Rubinstein, and P. L'Ecuyer, "The cross-entropy method for optimization," in *Handbook of statistics*. Elsevier, 2013, vol. 31, pp. 35–59.
- [55] G. Williams, P. Drews, B. Goldfain, J. M. Rehg, and E. A. Theodorou, "Aggressive driving with model predictive path integral control," in *2016 IEEE International Conference on Robotics and Automation (ICRA)*. IEEE, 2016, pp. 1433–1440.
- [56] C. Pinneri, S. Sawant, S. Blaes, J. Achterhold, J. Stueckler, M. Rolinek, and G. Martius, "Sample-efficient cross-entropy method for real-time planning," *arXiv preprint arXiv:2008.06389*, 2020.
- [57] R. Wang, J. Zhang, J. Chen, Y. Xu, P. Li, T. Liu, and H. Wang, "Dexgraspnet: A large-scale robotic dexterous grasp dataset for general objects based on simulation," 2023. [Online]. Available: <https://arxiv.org/abs/2210.02697>
- [58] X. Wang, B. Zhou, Y. Shi, X. Chen, Q. Zhao, and K. Xu, "Shape2motion: Joint analysis of motion parts and attributes from 3d shapes," in *Proceedings of the IEEE/CVF Conference on Computer Vision and Pattern Recognition*, 2019, pp. 8876–8884.
- [59] F. Xiang, Y. Qin, K. Mo, Y. Xia, H. Zhu, F. Liu, M. Liu, H. Jiang, Y. Yuan, H. Wang *et al.*, "Sapien: A simulated part-based interactive environment," in *Proceedings of the IEEE/CVF Conference on Computer Vision and Pattern Recognition*, 2020, pp. 11 097–11 107.
- [60] J. Huang, Y. Zhou, and L. Guibas, "Manifoldplus: A robust and scalable watertight manifold surface generation method for triangle soups," *arXiv preprint arXiv:2005.11621*, 2020.